Electrochemical Processing of Discrete Single-Walled Carbon Nanotube Anions

Stephen A. Hodge,[†] Siân Fogden,[†] Christopher A. Howard,[‡] Neal T. Skipper,[‡] and Milo S. P. Shaffer[†,*]

[†]Department of Chemistry, Imperial College London, London, SW7 2AZ, U.K. and [‡]Department of Physics and Astronomy, University College London, London, WC1E 6BT, U.K.

ABSTRACT The dissolution of single-walled carbon nanotubes (SWCNTs) remains a fundamental challenge, reliant on aggressive chemistry or ultrasonication and lengthy ultracentrifugation. In contrast, simple nonaqueous electrochemical reduction leads to spontaneous dissolution of individualized SWCNTs from raw, unprocessed powders. The intrinsic electrochemical stability and conductivity of these nanomaterials allow their electrochemical dissolution from a pure SWCNT cathode to form solutions of individually separate and distinct (*i.e.*, discrete) nanotube anions with varying charge density. The integrity of the SWCNT sp^2 framework during the charge/discharge process is demonstrated by optical spectroscopy data. Other than a reversible change in redox/solvation state, there is no obvious chemical functionalization of the structure, suggesting an analogy to conventional atomic electrochemical dissolution. The heterogeneity of as-synthesized SWCNT samples leads to the sequential dissolution of distinct fractions over time, with fine control over the electrochemical potential. Initial preferential dissolution of defective nanotubes and carbonaceous debris provides a simple, nondestructive means to purify raw materials without recourse to the usual, damaging, competitive oxidation reactions. Neutral SWCNTs can be recovered either by electroplating at an anode or by reaction with a suitable electrophile.

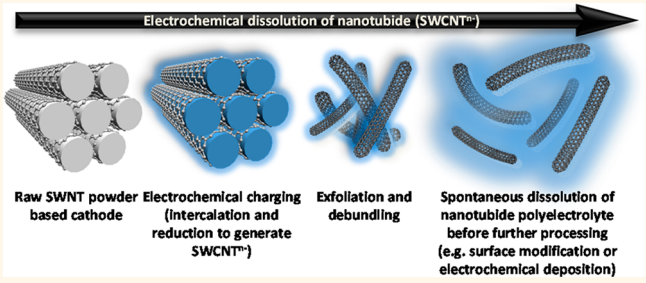

KEYWORDS: carbon nanotube · electrochemistry · dispersion · deposition · purification · functionalization

Single-walled carbon nanotubes (SWCNTs) typically form tightly bound, hexagonally packed "ropes" or "bundles", due to strong, attractive,[1] van der Waals (vdW) interactions (~0.5 eV nm^{-1}); these arrays do not form extended crystals due to entanglements and intrinsic heterogeneity in SWCNT length, diameter, and helicity distributions, but are nevertheless challenging to disperse or dissolve. Disassociating these bundles into individual SWCNTs is a critical step for both scientific studies and many applications, as well as for isolating pure sorted samples. Dispersions of individualized SWCNTs are generally produced using ultrasonication in either aqueous surfactant[2,3] or organic solvent[4,5] systems followed by ultracentrifugation. Initial ultrasonication causes SWCNT shortening and functionalization,[6,7] while (often repetitive) ultracentrifugation offers only very low yields. Neither step is well-suited for large-scale processing.

Spontaneous dissolution of SWCNTs is much rarer, but has been achieved chemically *via* the reduction of SWCNTs by sodium napthalide in tetrahydrofuran[8,9] or solvated electrons generated by sodium in liquid ammonia[10] and alternatively *via* the protonation of SWCNTs in chlorosulfonic acid.[11] Recent investigations of charge stoichiometry report the preferential dissolution of larger diameter SWCNTs at low charge: carbon ratios.[10,12] This article reports a new method for direct dissolution, purification, and potential sorting of commercially available as-received SWCNTs *via* a nonaqueous electrochemical procedure; remarkably, no prepurification processing is required. More generally, the approach highlights the possibility of electrochemical dissolution of discrete, well-defined nanoparticle ions, an approach that could be applied to a variety of electrochemically stable systems in the future; this perspective does not appear to have been explored

* Address correspondence to m.shaffer@imperial.ac.uk.

Received for review December 21, 2012 and accepted January 21, 2013.

Published online January 21, 2013
10.1021/nn305919p

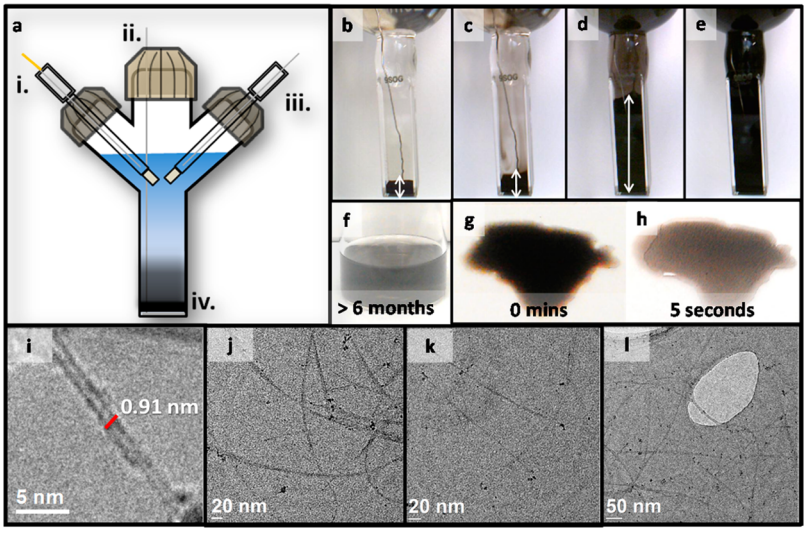

Figure 1. Electrochemical dissolution process. (a) Schematic illustration of the electrochemical process showing (i) Ag/Ag^+ reference electrode, (ii) Pt plate working electrode, (iii) Pt wire counter electrode, (iv) SWCNT powder. (b–e) Electrochemical dissolution of ~20 mg of raw HiPco SWCNT powder in 1 mM TBAP/DMF at −2.3 V over 5 days. The white arrows indicate the significant degree of swelling of the SWCNT powder bed. For smaller loadings (<10 mg), the dissolution process can be performed within 24 h, without agitation, to generate >1 mg mL^{-1} solutions (see movie in SI). (f) Under inert conditions the electrochemical dispersions were stable for several months. (g, h) Upon exposure to air, the dispersions in alkali-metal-based electrolytes were stable for only ≤5 s due to rapid charge-quenching/functionalization and subsequent reagglomeration. (i–l) TEM micrographs of electrochemically dispersed HiPco SWCNTs; the presence of individual SWCNTs and narrow bundles is apparent.

beyond the electrochemical synthesis of Zintl anion clusters produced *via* cathodic dissolution.[13]

Although the electrochemistry of molecular fullerenes is well-studied,[14] work on SWCNTs has relied on predispersed materials[15] or thin films[16] and focused on correlating electrode potentials to key spectroscopic features, measured *in situ*. Typically, relatively modest potentials have been applied in either aqueous[16] (typically −1.0 to +1.1 V (*vs* Ag/AgCl)) or occasionally organic[15] (±1.5 V (*vs* SCE)) electrolytes, resulting in bleaching of characteristic vis–nIR or nIR photoluminescence (PL) signals associated with electronic transitions between van Hove singularities (vHS) or corresponding resonant Raman features. Despite different apparent trends in Fermi energy in literature reports,[15–19] in general, redox potentials depend on nanotube diameter, with larger diameter SWCNTs reduced more favorably. Paolucci summarized three key difficulties with performing such spectroelectrochemical experiments: (1) high electrolyte concentration promotes flocculation of predispersed SWCNTs; (2) use of surfactants fouls the working electrodes, interfering with electrochemical data; (3) aqueous systems have a limited electrochemical stability window.[15] In view of such issues, this study uses dry, air-free, organic solvent-based electrolytic solutions to maximize the electrochemical stability window and avoid competing reactions or SWCNT functionalizations. Since the goal is dissolution, not accurate determination of redox potentials, a low supporting electrolyte concentration was selected to prevent SWCNT flocculation; the use of a dry powder as a starting material avoids surfactant. This redesign and repurposing of the electrochemical system enables a new phenomenon to emerge, the spontaneous electrochemical dissolution and plating of discrete nanoparticle ions; the effect raises interesting fundamental questions and is likely to be technologically useful.

RESULTS AND DISCUSSION

Electrochemical Dissolution of SWCNTs. As-received SWCNT powders were utilized without oxidative prepurifications, to avoid damaging the electronic properties. SWCNT powders were loaded into an electrochemical cell with three-electrode geometry (Figure 1a) and placed in contact with an energized platinum plate to form the working electrode; a protected platinum wire counter electrode, a Ag/Ag^+ reference electrode, and a suitable electrolyte were introduced as discussed below and in the Experimental Section.

Dissolution of the SWCNTs was not observed when the powder was left to sit in the electrolyte for several days; sonication produced only unstable dispersions. However, with the application of a constant potential of at least −1.6 V (*vs* Ag/Ag^+, *all potentials reported relative to this reference electrode*), black-colored trails were observed to leave the SWCNT electrode after a short period of time, without stirring, heating, or sonication. During this process, SWCNTs are charged and reduced to "nanotubide" species that spontaneously debundle and dissolve into the electrolyte due to electrostatic repulsion (where "nanotubide" is

the proposed term for a pure nanotube anion[10]). Between −1.6 and −2.0 V, overall dissolution is modest (∼5−20 wt %); on increasing potentials up to −2.3 V, 100 wt % dissolution was achieved for both HiPco and CoMoCAT SWCNTs. Overall, this complete electrochemical dissolution required ∼1 e^-/40−48 C atoms for HiPco SWCNTs and ∼1 e^-/20 C atoms for CoMoCAT SWCNTs. The figures assume that the integrated current indicates the SWCNTs charge (Figure S1); from fractionation experiments (below) and limiting currents, it is possible to estimate that no more than 10% of the total charge is consumed in other processes (electrolyte degradation or residual moisture). The charge ratios are in reasonable agreement with Penicaud[9] and Fogden,[10] who reported that purely chemical reductive dissolution of SWCNTs required 1 e^-/10−50 C atoms and 1 e^-/10 C atoms, respectively. The electrochemical reduction potentials required for SWCNT dissolution are significantly larger than applied to study spectroelectrochemical phenomena[15,16] due to the need for a high charge density, before dissolution. Using raw HiPco SWCNTs, concentrations exceeded 1.5 mg mL^{-1} in DMF, as determined by mass measurements.

The potentials required for dissolution did not vary with the specific electrolytic (salt or solvent) system used. *N*,*N*-Dimethylformamide (DMF) was the preferred solvent, on the basis of electrochemical stability and suitability for both neutral[20] and charged SWCNTs;[9] however, a range of electrochemically stable solvents, including propylene carbonate (PC), gave similar results (see SI, Figure S2 for a full list) provided that they were sufficiently dry (<10 ppm moisture content). Sodium tetraphenylborate (STPB), sodium perchlorate ($NaClO_4$), and tetrabutylammonium perchlorate (TBAP) were used predominantly, although other electrolytic salts (listed in the Experimental Section) were also tested. Nanotubide dissolution was not observed when electrolyte concentrations were >0.1 M, highlighting the formation of charge-stabilized colloidal systems that become destabilized at high counterion concentrations due to the contraction of the Debye screening length.[21] The typical electrolyte concentration used, 1 mM, corresponds to a Debye length of ∼6.7 nm in DMF[22] (ε = 36.7, 298 K). Upon exposure to atmospheric oxygen, charge quenching is expected to form tetrabutylammonium or alkali-metal (hydr)oxides upon the reduction of oxygen to superoxide by the highly reactive nanotubide species,[23] leading to reaggregation of the individualized neutral SWCNTs. However, other species such as H_2O/CO_2 may functionalize nanotubide surfaces. Electrochemical dispersions kept inside a glovebox were stable for more than 6 months (Figure 1f) with no visible aggregates; upon exposure to air, precipitation was observed within seconds for alkali-metal-based electrolytes (Figure 1g, h); in tetrabutylammonium (TBA^+) electrolytes, precipitation occurred over a few days, likely due to additional steric stabilization of the surfactant-like *n*-butyl chains. Direct sonication of SWCNTs in TBAP/DMF does not result in a stable dispersion.

Transmission electron microscopy (TEM) (Figure 1i-l) revealed that the fully dissolved material consisted predominantly of individualized SWCNTs, with some small bundles; high-speed ultracentrifugation (120000*g*, 6−24 h) of the nanotubide dispersions in DMF showed minimal sedimentation (see SI, Figure S3). Following charge quenching by exposure to clean, dry oxygen, UV−vis−nIR absorption and PL spectroscopy of both thin film and aqueous dispersions of electrochemically processed HiPco SWCNTs showed characteristic vHS features. These optical spectroscopic techniques are particularly sensitive to defects and surface modifications due to the relatively long exciton diffusion length in SWCNTs;[24] the similarity of the spectra to those obtained from the unprocessed starting material (see SI, Figure S4) confirmed the absence of further defects or functionalization of the SWCNTs during electrochemical processing.

SWCNT Purification. The quality of the dispersed material was studied by observing changes in the intensities of the G [1500−1600 cm^{-1}] and D [1200−1400 cm^{-1}] peaks in the Raman spectra (Figure 2a, b), which are characteristic of structural order and disorder, respectively.[25] The defect concentration in the fractions dissolved at less reducing potentials was significantly greater than that in the raw material (as indicated by an increased peak intensity ratio, I_D/I_G). The defect concentration in the undissolved material was correspondingly lower, suggesting a separation on the basis of purity; the effect is strong, in some cases, offering a factor of 2 improvement in I_D/I_G ratio. The result rules out ongoing functionalization as a primary dissolution mechanism; rather, impurities such as amorphous carbons, graphitic (metal-containing) nanoparticles, and short/defective SWCNTs are reduced preferentially. The mechanism is not primarily dependent on diffusion rates, as electrochemical dissolution at mild potentials does not lead to the progressive dissolution of purer SWCNTs over time; these species require significantly increased charge densities, available at greater reducing potentials. The purification trends were confirmed with TEM (Figure 2d) and TGA (see SI, Figure S5). In sequential dissolutions, at increasingly more reducing potentials, fractions contained significantly lower amounts of amorphous, graphitic, and metal catalyst debris; after electrochemical treatment, both HiPco and CoMoCAT powders showed an increased peak combustion temperature and lower residual metal content in the undissolved fraction. This removal of amorphous carbons and other impurities provides a new purification route for raw SWCNT powders, an alternative to more conventional, but destructive, oxidation and/or sonication treatments.[26] A useful strategy is to run the process at −2.0 V to dissolve the majority of impurities

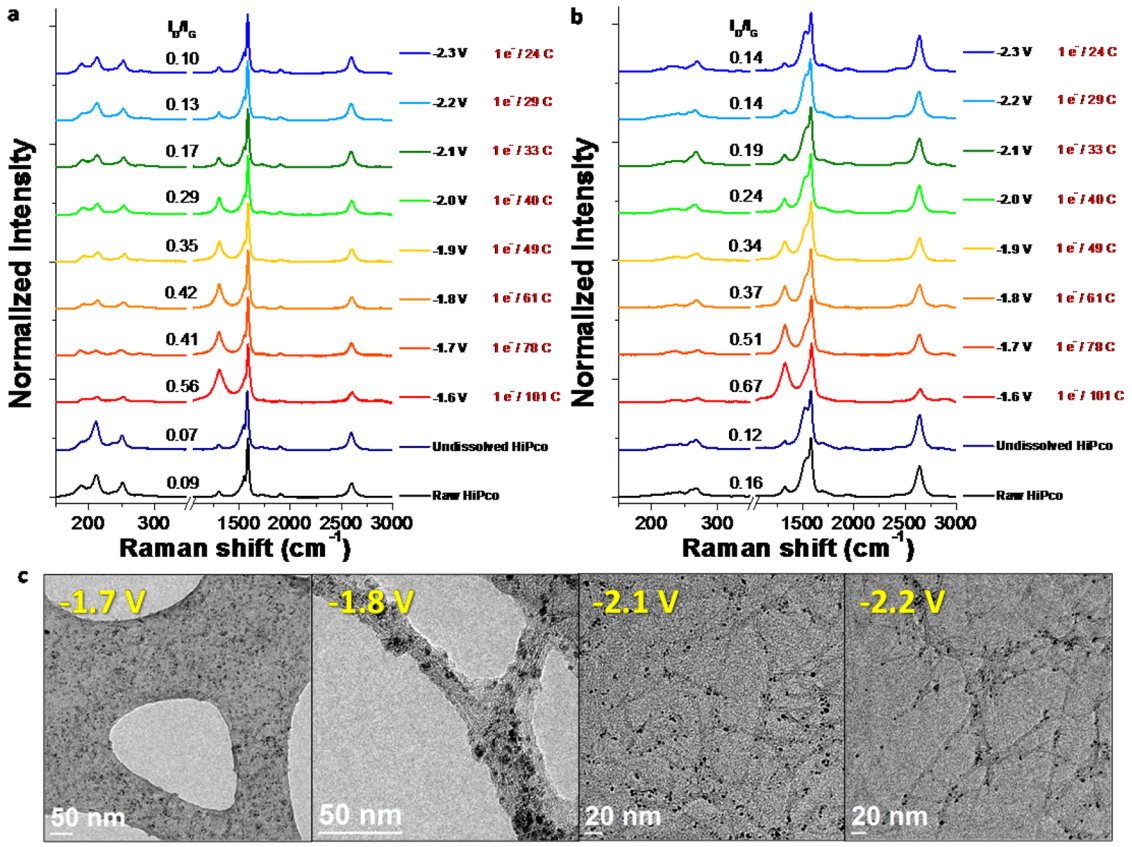

Figure 2. Sequential dissolutions of raw HiPco SWCNT powder in 1 mM STPB/DMF. Following each step the majority of the nanotubide dispersion was removed and fresh electrolyte (containing ~5−10 ppm water) added. (a, b) Raman analysis of the raw, undissolved, and electrochemically dispersed HiPco fractions at sequential reduction potentials using E_{laser} = 1.96 and 2.33 eV, respectively. Each spectrum is an average of 5 scans at different positions. Intensities are normalized to the G peak. (c) TEM images of selected nanotubide fractions showing the preferential dissolution of metallic and carbonaceous debris (−1.6 to −2.0 V) followed by the progressive dissolution of purer individualized SWCNT material (>−2.0 V).

(~20 wt %), followed by a dissolution of the purer material at −2.3 V. During the sequential dissolution experiments, Raman radial breathing modes (Figure 2a, b) showed no significant selectivity for SWCNT diameter or electronic type. This outcome may not be surprising: the bundled nature of the starting material will tend to trap a mixture of SWCNTs until all species are sufficiently charged to be mobile.

Electrochemical Dissolution Mechanisms. The nanotubide dissolution process is driven by the intercalation of the background electrolyte and solvent into the SWCNT powder electrode to balance the electronic charge introduced at reducing potentials. During these processes, which correlate with capacitive charging of the SWCNT network (Figure 3), the powder swells significantly (Figure 1b−e); as electrostatic interactions overcome the attractive intertube vdW forces, the SWCNT network exfoliates and debundles. Diffusion of the charged species away from the electrode generates a charged polyelectrolyte nanotubide solution. Electrochemical double-layer charging is frequently exploited in SWCNT capacitors[27] and electromechanical actuators,[28] with actuation caused by expansion due to charging, but without obtaining dissolution; large capacitive charging signals were observed for all SWCNTs in different electrolytes during cyclic voltammetry (CV) experiments. Increasing capacitance at more reducing potentials has previously been attributed to sequential electron doping of the semiconducting SWCNTs.[29−31] Very recently,[32] specific vHS features ((*17,3*) HOMO/LUMO energies) were assigned to CV features, using Meijo SWCNTs; metallic SWCNTs on the other hand showed purely capacitive behavior. The CV experiments presented here for HiPco SWCNTs (Figure 3a) also reveal the appearance of broad features below ~−0.5 V rather than a single redox wave, which can be attributed to the (un)doping of the large number of distinct (*n,m*) species that are present. At such slow scan rates (<0.5 mV s^{-1}), reductive debundling and dissolution is followed by reaggregation (rebundling) on the reverse cycle. At fixed reducing potentials, the charge density is high enough and the electrolyte concentration low enough that an electrostatically stabilized colloid forms. The spontaneous nature of the dissolution confirms that the process is thermodynamically favored, with a lower enthalpy of dissolution than for a neutral SWCNT system.[23]

The initiation time (defined as the first observation of black trails diffusing away from the SWCNT powder

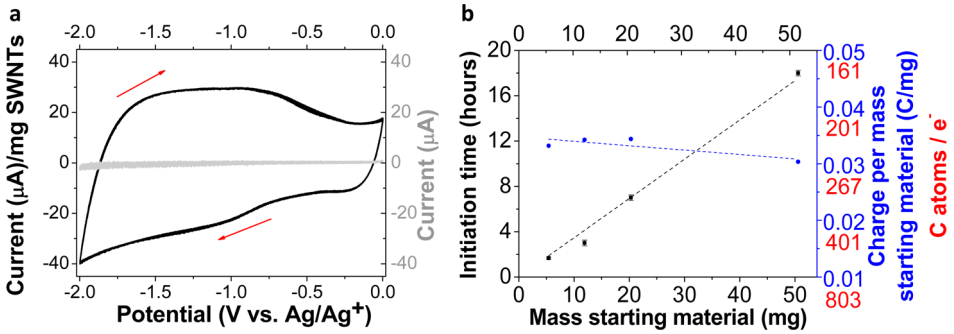

Figure 3. Electrochemical dissolution mechanisms. (a) Cyclic voltammogram of a HiPco SWCNT powder electrode in 0.1 M STPB/DMF, scan rate 0.5 mV s^{-1}, 5 cycles (black), and the respective control CV of a Pt wire and plate working electrode with no SWCNTs present (gray). Arrows indicate the direction of scan. (b) Initiation time (squares) and the charge required (circles) for the electrochemical dissolution of raw HiPco SWCNTs with increasing amounts of starting material (−2.3 V, 1 mM TBAP/DMF electrolyte).

electrode) varied between SWCNT batch and manufacturer, but was linked to charging of the entire powder. The charge passed before first observed dissolution (Figure 3b) was consistently ~0.03 C mg^{-1} SWCNT (1 e^-/270 C atoms), independent of starting mass, for raw HiPco powder; this charging threshold varies between SWCNT batch or material (*e.g.*, CoMoCAT ~0.08 C mg^{-1}, 1 e^-/100 C atoms). For the HiPco powder used, accumulation of charge equates to a gravimetric capacitance of 13 F g^{-1}. The value is similar to the capacitance of highly pure HiPco SWCNT electrodes in 1 M $LiClO_4$/PC electrolyte (45 F g^{-1}),[33] but lower due to low electrolyte concentration and a significantly higher fraction of amorphous carbon in the raw powder. In addition, the larger size of TBA^+ ions compared to Li^+ inherently produces a lower gravimetric capacitance, due to steric effects at the interface.[34] After the initiation period, the concentration of dissolved SWCNTs increases with time, eventually reaching a plateau that defines a process yield; larger SWCNT loadings generated a higher absolute mass dissolved. However, the yield appeared limited by slower kinetics, inherently linked to the depth of the electrode powder bed; the lack of any agitation limits nanotubide motion to primarily diffusive effects. The maximum dissolved yield from a given SWCNT sample will depend on physical parameters such as nanotube length, entanglement, and density, as well as electronic effects including band structure and connectivity; since amorphous carbon and particulates dissolve preferentially, they can increase the apparent yield. The electrochemical cell geometry also plays a key role. The present cell was designed for proof of concept studies; future redesigns can be adapted for bulk processing, maximizing yields and concentrations with the use of thinner electrodes and short diffusion distances.

During fixed potential dissolution experiments, widely used materials, HiPco and CoMoCAT SWCNTs (typically ~0.1−1 μm long, as observed by AFM), displayed similar electrochemical dissolution behavior, providing nanotubide concentrations of >1 mg mL^{-1}; significantly longer Hanwha,[35] Meijo (~1−5 μm), and Supergrowth[36] (100−300 μm, as observed by scanning electron microscopy (SEM)) materials showed dissolution of significantly smaller concentrations (<0.1 mg mL^{-1}) at equivalent time points. Given that the persistence length of SWCNTs is on the order of micrometers,[37] and possibly higher when charged, the motion of long SWCNTs should be highly restricted; very long charged SWCNTs may remain trapped within the working electrode or dissolve at very low concentrations due to a percolation limit.[38] Assuming that electrical percolation within the dispersed nanotubes is avoided due to electrostatic repulsion, the ultimate concentration limit should be defined by the type of complex phase diagram, identified for protonated SWCNTs in superacid.[39,40] If so, higher fractional electrochemical charge (~1 e^-/12 C atoms), if attained without disconnection, should offer the opportunity to form nematic phases.

Nanotubide Functionalization and Electrochemical Deposition. There are a number of convenient onward processing options for the SWCNT anions produced electrochemically. They can either be quenched in pure, dry oxygen, to regenerate neutral, unfunctionalized SWCNTs with their original (opto)electronic properties (SI, Figure S4), or deliberately derivatized using a whole library of useful and versatile reactions developed for chemically generated nanotubides.[41] Figure 4 shows a simple dodecyl grafting of reduced CoMoCAT SWCNTs (1 e^-/20 C atoms) using 1-iodododecane, giving a degree of functionalization of ~1 dodecyl chain/58 C atoms. The grafting efficiency (charge utilization) is relatively high compared to chemical reduction routes that typically employ excess alkali metal:carbon stoichiometry (for example ~1 dodecyl chain/13 C atoms for 5 Na^+/C atom).[42] By ensuring that the SWCNTs are individually dissolved before reaction, the degree of functionalization and permanent debundling can be maximized. The negative charge can also be removed electrochemically *via* the electrodeposition of SWCNTs onto various conductive electrode

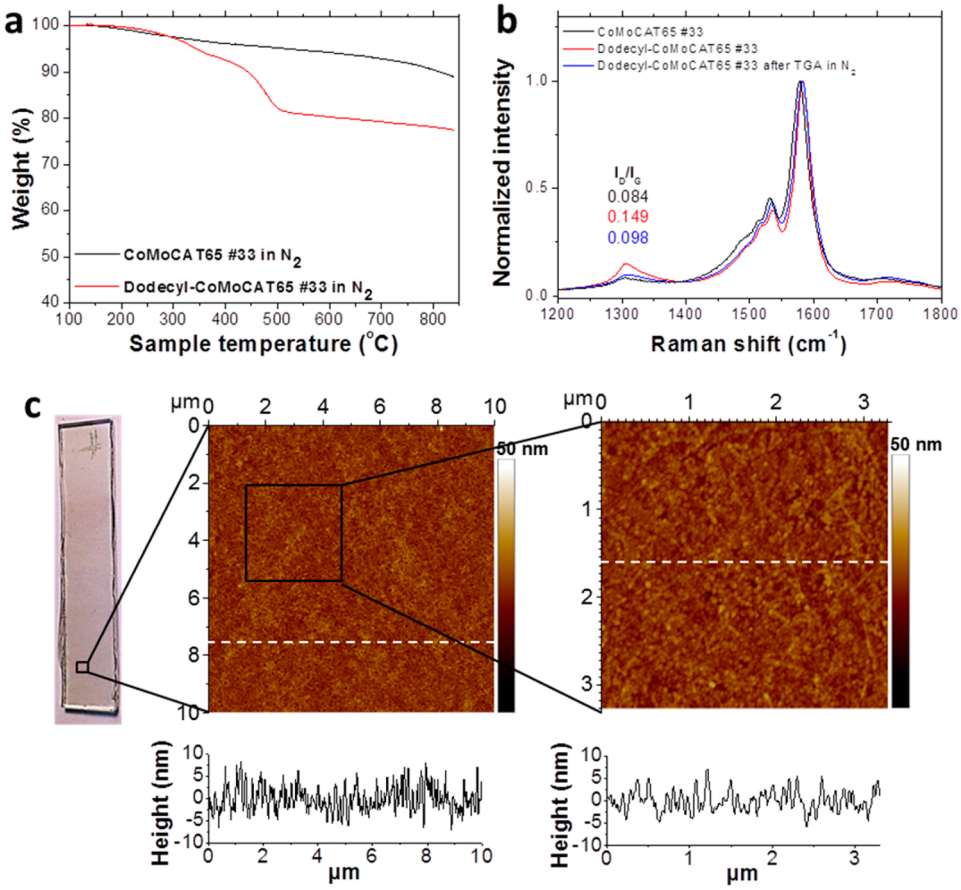

Figure 4. Nanotubide functionalization. (a) TGA of as-received and dodecyl-grafted SWCNTs in an inert atmosphere. (b) Raman spectra of dodecyl-grafted and the ungrafted SWCNTs following TGA under N_2 using E_{laser} = 2.33 eV. (c) Photograph (left) and AFM height micrographs (right) and height profiles (below) of an electrochemically deposited film of HiPco SWCNTs on an ITO-glass electrode at −1.4 V, 24 h, showing relatively large area, highly uniform SWCNT network deposition. White dashed lines relate to the measured height profiles of the SWCNT film.

materials (*e.g.*, pure metals, metallic/conductive thin films). Transparent-conductive electrodes (*e.g.*, ITO-glass, Figure 4c and Figure S6c−e) are particularly useful due to the ease of subsequent characterization (Raman, thin film UV−vis−nIR, and PL spectroscopies, SEM, AFM) directly on the electrode surface.

As for the dissolution process, electrodepositions were performed at constant potential; the platinum plate electrode was typically swapped for an ITO-glass electrode, and sequential depositions were performed at increasingly oxidizing potentials from −2.0 to −1.0 V (+0.1 V increments, 48 h at each step). At more oxidizing potentials than −1.0 V, the remaining SWCNTs reaggregated. The geometry of the current electrochemical cell and the slow diffusion of long SWCNTs limited the deposits obtained to low thickness (~97% transmittance); thicker films with more uniform morphologies of individualized SWCNTs could be improved with cell redesign, finer potential control, and the addition of brighteners to enhance deposition quality. However, the type of brighteners widely used for traditional electrodeposition will need to be redesigned for the electrodeposition of nanotube anions.

Once all the SWCNTs are solubilized as individual ions, selective electrodeposition at well-defined electrode potentials holds more promise for a scalable route to separation of distinct SWCNTs than the dissolution step. Existing methods for the separation[43−50] of SWCNTs based on electronic character or helicity rely on sonication and/or centrifugation, severely limiting fundamental scalability; batch scale chemical charging involves the consumption of expensive and difficult reagents. In the current preliminary experiments, weak diameter selectivity was observed by Raman during ongoing electrodeposition, encouraging further development efforts to limit the entanglement of unwanted SWCNTs in successfully electrodeposited networks. In principle, selective electrochemical processing of individualized nanotubide ions may offer a scalable route for separation by diameter, helicity, or electronic character, vital for many applications such as transparent conductive films and nanoelectronic components. While there are some quantitative inconsistencies in the literature data for the first redox potentials of SWCNTs,[51] the dependence on key SWCNT characteristics is encouraging. On the other hand, the multiple

charging events required for dissolution require further theoretical consideration; the differences between different SWCNT types may become blurred at higher charge densities, and dielectric effects, for example, may be important.

CONCLUSIONS

This study describes a new approach for the formation and dissolution of discrete nanotube anions that will generalize to other electrochemically stable nanoparticles. While the SWNT anions are still polydispersed, each individual species retains its integrity and identity. Common, commercial, as-received SWCNT powders were fully dissolved using a mild electrochemical reduction in nonaqueous electrolytic solutions without the use of ultrasonication, ultracentrifugation, covalent modification, or strongly bound wrapping agents. The electrochemical aproach offers much greater control over reduction potential than chemical charging routes that use specific reductants or charge transfer agents; the charging current allows independent control of charge:carbon stoichiometry more directly and conveniently than, for example, adjusting the alkali metal:carbon ratio.[12,52] Careful control of the electrochemical potential removes carbonaceous impurities, providing a nondestructive strategy for SWCNT purification. Three different approaches can be used to quench the charge on nanotubide ions: exposure to clean, dry oxygen, deliberate derivatization, or electrochemical quenching *via* depositions. Electrodeposition provides a high level of control and a variety of new processing options.

The dissolution and purification technique has been demonstrated at the tens of milligram scale, but offers considerable promise for scaling to larger quantities, while avoiding inconvenient reagents such as superacids, liquid ammonia, or alkali metals. Although the current system is only a proof-of-concept, electrochemical processes are widely used industrially for bulk purification and extraction, including in controlled atmospheres; aluminum electrowinning is, for example, performed in an air-free, nonaqueous electrolytic system.[53] Ultimately, once larger scale cells are optimized, SWNT processing may be scaled out to a battery of multiple cells, in a manner analogous to other commercial processes. By combining dissolution with electroplating, a semicontinuous bulk purification process can be envisioned for nanotubes, in a similar fashion to the industrial purification of copper.[54] This approach may provide a route toward large-scale sorting of specific SWCNT species (each representing a distinct molecular structure), which almost always coexist as-synthesized, despite recent advances.[55] In the future, nanotubide solutions monodispered in structure and charge density may, therefore, be prepared.

Fundamentally, the generalization of this approach to the dissolution of purified nanoparticle ions will allow specific charge density to be investigated with charged nanoparticles dispersed as discrete objects. To apply this electrochemical approach, particles must be electrochemically stable and reasonably electrically conductive. Possible examples include multiwalled carbon nanotubes (MWCNTs), graphenes, and other conductive nanopowders (such as noble metals); preliminary experiments show promising results for MWCNTs (see SI, Figure S7). Understanding the electrochemistry of nanoparticle ions will require new methods and theory, since multiple redox events are involved at a range of potentials related to the complex density of states defined by the particle composition, size, and dimensionality. These studies will be enabled by the availability of more monodispersed samples, *via* the electrochemical process itself or otherwise. The development of electrochemical routes for purification and assembly of nanomaterials will, thus, enable both fundamental studies and new applications.

EXPERIMENTAL SECTION

Materials. HiPco SWCNTs (batches R0550, R0448; Carbon Nanotechnologies Inc., USA), CoMoCAT SWCNTs (batches SG0000002, SG0000033; SWeNT, USA), CarboLex (AP-grade; CarboLex Inc., USA), Hanwha SWCNTs (batch ASA-100F: A-091230-2; Hanwha Nanotech Corp., South Korea), and Supergrowth SWCNTs (batch STD2; AIST, Japan) were used as-received without any pretreatments. DMF (anhydrous, 99.8%), DMA (anhydrous, 99.8%), 1-methyl-2-pyrrolidinone (anhydrous, 99.5%), 1,3-dimethyl-2-imidazolidinone (puriss., absolute, over molecular sieve ($H_2O \leq 0.04\%$), $\geq 99.5\%$), propylene carbonate (anhydrous, 99.7%), dimethyl sulfoxide (anhydrous, $\geq 99.9\%$), acetonitrile (anhydrous, 99.8%), and 1,2-dimethoxyethane (anhydrous, 99.5%) were all purchased from Sigma-Aldrich and used as-received. 1-Cyclohexyl-2-pyrrolidone (99%) was also purchased from Sigma-Aldrich, but further dried by vacuum distillation over molecular sieves. Tetrahydrofuran was dried in-house in a solvent-drying tower packed with alumina. The anhydrous electrolytic salts used throughout the research (tetrabutylammonium perchlorate, sodium tetraphenylborate, sodium perchlorate, tetrabutylammonium tetraphenylborate, lithium perchlorate) were all purchased from Sigma-Aldrich and used as-received. Electrolytic solutions were further dried by 3 Å molecular sieves and kept in a glovebox.

Electrochemical Cell Setup. Electrochemical cells were custom designed and produced by an in-house glassblower. A small-volume cell (7 mL) comprised a 10 mm path length Pyrex cuvette with four screw-neck threads for electrode insertion and connection to a Schlenk line. A larger volume cell (30 mL) was also made by combining a Pyrex cuvette and a three-necked round-bottom flask. The pyrex cuvettes were purchased from Starna Scientific Ltd., UK. The electrochemical cell was either attached to a Schlenk apparatus or manipulated in an mBraun Labmaster SP glovebox. For experiments using the Schlenk apparatus, the SWCNT powder and electrolytic salt were dried under vacuum at 190 °C followed by three freeze–thaw cycles with zero-grade nitrogen (BOC gases, UK, 99.998% purity). Anhydrous DMF was added using a dry, air-free syringe. During Schlenk experiments, a positive pressure of nitrogen gas was maintained in the cell to minimize the entry of oxygen and

moisture. For experiments using the glovebox, SWCNTs were dried using the above procedure and placed into the glovebox, and the electrochemical cell was kept sealed throughout the experiments in case of glovebox contamination. Levels of moisture and oxygen were <1 ppm throughout the duration of all electrochemical experiments.

If required, SWCNT powders were ground before the drying procedure using a pestle and mortar for 5−10 min to improve electrode connectivity and placed at the bottom of the electrochemical cell, on top of a 10 mm^2 piece of platinum foil attached to a platinum wire. After the reaction, the dissolved SWCNT supernatant was removed from the electrochemical cell by air-free syringe or cannula techniques. The reference electrode, Ag/Ag^+ (IJ Cambria Scientific, UK), contained 0.01 M silver nitrate and 0.1 M TBAP in acetonitrile. A porous glass frit protected platinum wire counter electrode was used throughout to ensure no byproducts entered the working electrode compartment. The counter electrode compartment contained ~1−2 M electrolytic salt/DMF.

SWCNT Functionalization. 1-Iodododecane (0.3 mL, 1.22 mmol) was added to 1 mL of CoMoCAT SWCNTs (0.9 mg mL^{-1}) that were electrochemically dissolved to ~1 charge/20 C atoms in 1 mM $NaClO_4$/DMF and stirred for 24 h. The resulting gel-like product was filtered onto a PTFE membrane (0.025 μm) under vacuum, washed with chloroform (50 mL) and water (50 mL), dried, and removed from the filter membrane. The product was further soaked in water (72 h) and chloroform (72 h) with additional stirring, filtered onto a PTFE membrane, and recovered.

Characterization. A Solartron 1250 potentiostat (Solartron Analytical, UK) was used for electrochemical measurements using CorrWare 2 software.

Raman spectra of powder/drop-casted samples were obtained with a LabRAM Infinity instrument (Horiba Jobin-Yvon Ltd.) with a 633 nm He−Ne laser (1.96 eV) and 532 nm Nd:YAG laser (2.33 eV). All Raman spectra were recorded using a grating of 1800 grooves mm^{-1}. The maximum powers of the 633 and 532 nm lasers at the sample were 8 and 24 mW, respectively. The laser power was varied to ensure no damage to samples; typically, 100% intensity was used for the 633 nm laser and 25% intensity for the 532 nm laser. Samples were measured either in raw powder form, as drop-casted dispersions on glass microscope slides, or as electrodeposited films on various electrode surfaces. At least five consistent spectra were measured for each sample at different locations to reduce the effect of sample heterogeneity.

Transmission electron microscopy was carried out using a JEOL2010 TEM at 200 kV operating voltage. Samples were typically prepared on 300 copper mesh holey carbon grids (Agar Scientific) by drop-casting onto the grid supported by a filter paper and left to dry in a nitrogen-filled glovebox for several days. Samples were removed from the glovebox, washed on filter paper with 2−3 drops of DMF, acetonitrile, or water to remove electrolytic salts, and then further washed with IPA.

Scanning electron microscopy was performed using a Leo Gemini 1525 high resolution field emission gun scanning electron microscope (FEGSEM) using SmartSEM software. ITO-glass electrodes were affixed onto aluminium sample stubs using carbon tabs (Agar Scientific Ltd., U.K.). MWCNT dispersions were drop-casted directly onto clean silica substrates and washed to remove electrolytic salts.

Atomic force microscopy (AFM) was carried out using a Nanoscope IV Digital Instruments AFM (Veeco) on ITO-glass substrates with SWCNT electrodeposit. Samples were washed with DMF and water, and dried in air.

UV−vis−nIR spectroscopy was carried out using a Lambda 950 spectrophotometer (Perkin-Elmer). Photoluminescence spectroscopy was performed using a Nanospectralyzer NS1 (Applied NanoFluorescence). Samples were prepared either in 1 wt % sodium deoxycholate/D_2O by ultrasonication and ultracentrifugation or as thin films on glass substrates by dispersion drop-casting. Concentrations of electrochemically dissolved SWCNTs were measured predominantly by mass measurements, following extensive washing to remove electrolytic salts. Optical absorbance measurements using a typical SWCNT extinction coefficient[56] (3264 mL mg^{-1} m^{-1} @ 660 nm) were found to be consistent with mass measurements and were used at low concentrations. For optical measurements of SWCNT concentrations as high as 1.5 mg mL^{-1}, dilution is required. However, the introduction of fresh DMF (containing ~5−10 ppm water) leads to some degree of charge quenching/functionalization, and hence measurement inaccuracy; therefore, mass measurements were preferred at higher concentrations.

Ultracentrifugation was carried out using a Beckmann Coulter Optima L-90K with swinging bucket rotor (SW-41Ti) using polyallomer centrifugation tubes.

Thermogravimetric analysis (TGA) was carried out using a Perkin-Elmer Pyris 1 TGA. TGA cycles performed in an N_2 atmosphere (flow rate: 60 mL min^{-1}) were heated from 50 °C to 100 °C at 10 °C min^{-1}, then held isothermally for 30 min to remove residual water/DMF. The temperature cycle was then ramped from 100 °C to 850 °C at 10 °C min^{-1}.

Water contents of electrolytes were measured using Karl Fischer titration conducted with a Mettler Toledo DL32 coulometer using HYDRANAL-Coulomat AD reagent (Sigma-Aldrich).

Conflict of Interest: The authors declare the following competing financial interest(s): Additional support for this project was provided by Linde North America Inc. to whom associated patent filings have been licensed, where S.F. is currently employed, and for whom the other authors consult.

Supporting Information Available: Further characterization of electrochemically dissolved/deposited materials (Figures S1−S7 and movie file). This material is available free of charge *via* the Internet at http://pubs.acs.org.

Acknowledgment. The authors would like to thank Mr. Wilf Corrigan (LSI Logic Corporation, USA) and EPSRC EP/G007314/1 for the funding of this project. The authors would like to thank Ms. Charlene Lawton (Raman), Mr. David B. Anthony (SEM), Mr. Hin-Chun Yau (AFM), Mr. Stephen Ramsey (in-house glass blowing), and Dr. Kenji Hata (AIST, Japan) for providing Supergrowth SWCNTs.

REFERENCES AND NOTES

1. Girifalco, L. A.; Hodak, M.; Lee, R. S. Carbon Nanotubes, Buckyballs, Ropes and a Universal Graphitic Potential. *Phys. Rev. B* **2000**, *62*, 13104–13110.
2. Moore, V. C.; Strano, M. S.; Haroz, E. H.; Hauge, R. H.; Smalley, R. E.; Schmidt, J.; Talmon, Y. Individually Suspended Single-Walled Carbon Nanotubes in Various Surfactants. *Nano Lett.* **2003**, *3*, 1379–1382.
3. O'Connell, M. J.; Bachilo, S. M.; Huffman, C. B.; Moore, V. C.; Strano, M. S.; Haroz, E. H.; Rialon, K. L.; Boul, P. J.; Noon, W. H.; Kittrell, C.; *et al*. Band Gap Fluorescence from Individual Single-Walled Carbon Nanotubes. *Science* **2002**, *297*, 593–596.
4. Furtado, C. A.; Kim, U. J.; Gutierrez, H. R.; Pan, L.; Dickey, E. C.; Eklund, P. C. Debundling and Dissolution of Single-Walled Carbon Nanotubes in Amide Solvents. *J. Am. Chem. Soc.* **2004**, *126*, 6095–6105.
5. Bergin, S. D.; Nicolosi, V.; Streich, P. V.; Giordani, S.; Sun, Z.; Windle, A. H.; Ryan, P.; Niraj, N. P. P.; Wang, Z.-t. T.; Carpenter, L.; *et al*. Towards Solutions of Single-Walled Carbon Nanotubes in Common Solvents. *Adv. Mater.* **2008**, *20*, 1876–1881.
6. Lu, K.; Lago, M.; Chen, Y. K.; Green, M. L. H.; Harris, P. J. F.; Tsang, S. C. Mechanical Damage of Carbon Nanotubes by Ultrasound. *Carbon* **1996**, *34*, 814–816.
7. Vichchulada, P.; Cauble, M. A.; Abdi, E. A.; Obi, E. I.; Zhang, Q.; Lay, M. D. Sonication Power for Length Control of Single-Walled Carbon Nanotubes in Aqueous Suspensions Used for 2-Dimensional Network Formation. *J. Phys. Chem. C* **2010**, *114*, 12490–12495.
8. Anglaret, E.; Dragin, F.; Pénicaud, A.; Martel, R. Raman Studies of Solutions of Single-Wall Carbon Nanotube Salts. *J. Phys. Chem. B* **2006**, *110*, 3949–3954.
9. Pénicaud, A.; Poulin, P.; Derré, A.; Anglaret, E.; Petit, P. Spontaneous Dissolution of a Single-Wall Carbon Nanotube Salt. *J. Am. Chem. Soc.* **2005**, *127*, 8–9.

10. Fogden, S.; Howard, C. A.; Heenan, R. K.; Skipper, N. T.; Shaffer, M. S. P. Scalable Method for the Reductive Dissolution, Purification, and Separation of Single-Walled Carbon Nanotubes. *ACS Nano* **2011**, *6*, 54–62.
11. Parra-Vasquez, N. G.; Behabtu, N.; Green, M. J.; Pint, C. L.; Young, C. C.; Schmidt, J.; Kesselman, E.; Goyal, A.; Ajayan, P. M.; Cohen, Y.; *et al*. Spontaneous Dissolution of Ultralong Single- and Multiwalled Carbon Nanotubes. *ACS Nano* **2010**, *4*, 3969–3978.
12. Voiry, D.; Drummond, C.; Penicaud, A. Portrait of Carbon Nanotube Salts as Soluble Polyelectrolytes. *Soft Matter* **2011**, *7*, 7998–8001.
13. Warren, C. J.; Haushalter, R. C.; Bocarsly, A. B. The Electrochemical Synthesis of Telluride Zintl Anions. *J. Alloys Compd.* **1995**, *229*, 175–205.
14. Dubois, D.; Moninot, G.; Kutner, W.; Jones, M. T.; Kadish, K. M. Electroreduction of Buckminsterfullerene, C_{60}, in Aprotic Solvents. Solvent, Supporting Electrolyte, and Temperature Effects. *J. Phys. Chem.* **1992**, *96*, 7137–7145.
15. Paolucci, D.; Franco, M. M.; Iurlo, M.; Marcaccio, M.; Prato, M.; Zerbetto, F.; Pénicaud, A.; Paolucci, F. Singling Out the Electrochemistry of Individual Single-Walled Carbon Nanotubes in Solution. *J. Am. Chem. Soc.* **2008**, *130*, 7393–7399.
16. Tanaka, Y.; Hirana, Y.; Niidome, Y.; Kato, K.; Saito, S.; Nakashima, N. Experimentally Determined Redox Potentials of Individual *(n,m)*Single-Walled Carbon Nanotubes. *Angew. Chem.* **2009**, *48*, 7655–7659.
17. Hirana, Y.; Tanaka, Y.; Niidome, Y.; Nakashima, N. Strong Micro-Dielectric Environment Effect on the Band Gaps of *(n,m)*Single-Walled Carbon Nanotubes. *J. Am. Chem. Soc.* **2010**, *132*, 13072–13077.
18. Okazaki, K.; Nakato, Y.; Murakoshi, K. Absolute Potential of the Fermi Level of Isolated Single-Walled Carbon Nanotubes. *Phys. Rev. B* **2003**, *68*, 35434–35434.
19. O'Connell, M. J.; Eibergen, E. E.; Doorn, S. K. Chiral Selectivity in the Charge-Transfer Bleaching of Single-Walled Carbon-Nanotube Spectra. *Nat. Mater.* **2005**, *4*, 412–418.
20. Bergin, S. D.; Sun, Z.; Rickard, D.; Streich, P. V.; Hamilton, J. P.; Coleman, J. N. Multicomponent Solubility Parameters for Single-Walled Carbon Nanotube−Solvent Mixtures. *ACS Nano* **2009**, *3*, 2340–2350.
21. Israelachvili, J. *Intermolecular and Surface Forces*, second ed.; Academic Press: San Diego, CA, 1991.
22. Lund, H.; Hammerich, O. *Organic Electrochemistry*; M. Dekker: New York, 2001.
23. Catheline, A.; Valles, C.; Drummond, C.; Ortolani, L.; Morandi, V.; Marcaccio, M.; Iurlo, M.; Paolucci, F.; Penicaud, A. Graphene Solutions. *Chem. Commun.* **2011**, *47*, 5470–5472.
24. Cognet, L.; Tsyboulski, D. A.; Rocha, J.-D. R.; Doyle, C. D.; Tour, J. M.; Weisman, R. B. Stepwise Quenching of Exciton Fluorescence in Carbon Nanotubes by Single-Molecule Reactions. *Science* **2007**, *316*, 1465–1468.
25. Dresselhaus, M. S.; Dresselhaus, G.; Saito, R.; Jorio, A. Raman Spectroscopy of Carbon Nanotubes. *Phys. Rep.* **2005**, *409*, 47–99.
26. Park, T.-J.; Banerjee, S.; Hemraj-Benny, T.; Wong, S. S. Purification Strategies and Purity Visualization Techniques for Single-Walled Carbon Nanotubes. *J. Mater. Chem.* **2006**, *16*, 141–154.
27. Signorelli, R.; Ku, D. C.; Kassakian, J. G.; Schindall, J. E. Electrochemical Double-Layer Capacitors Using Carbon Nanotube Electrode Structures. *Proc. IEEE* **2009**, *97*, 1837–1847.
28. Baughman, R. H.; Cui, C.; Zakhidov, A. A.; Iqbal, Z.; Barisci, J. N.; Spinks, G. M.; Wallace, G. G.; Mazzoldi, A.; De Rossi, D.; Rinzler, A. G.; *et al*. Carbon Nanotube Actuators. *Science* **1999**, *284*, 1340–1344.
29. Kimizuka, O.; Tanaike, O.; Yamashita, J.; Hiraoka, T.; Futaba, D. N.; Hata, K.; Machida, K.; Suematsu, S.; Tamamitsu, K.; Saeki, S.; *et al*. Electrochemical Doping of Pure Single-Walled Carbon Nanotubes Used as Supercapacitor Electrodes. *Carbon* **2008**, *46*, 1999–2001.
30. Ruch, P.; Hardwick, L.; Hahn, M.; Foelske, A.; Kotz, R.; Wokaun, A. Electrochemical Doping of Single-Walled Carbon Nanotubes in Double Layer Capacitors Studied by *in Situ* Raman Spectroscopy. *Carbon* **2009**, *47*, 38–52.
31. Yamada, Y.; Tanaka, T.; Machida, K.; Suematsu, S.; Tamamitsu, K.; Kataura, H.; Hatori, H. Electrochemical Behavior of Metallic and Semiconducting Single-Wall Carbon Nanotubes for Electric Double-Layer Capacitor. *Carbon* **2012**, *50*, 1422–1424.
32. Al-zubaidi, A.; Inoue, T.; Matsushita, T.; Ishii, Y.; Hashimoto, T.; Kawasaki, S. Cyclic Voltammogram Profile of Single-Walled Carbon Nanotube Electric Double-Layer Capacitor Electrode Reveals Dumbbell Shape. *J. Phys. Chem. C* **2012**, *116*, 7681–7686.
33. Shiraishi, S.; Kurihara, H.; Okabe, K.; Hulicova, D.; Oya, A. Electric Double Layer Capacitance of Highly Pure Single-Walled Carbon Nanotubes (HiPco(TM) Buckytubes(TM)) in Propylene Carbonate Electrolytes. *Electrochem. Commun.* **2002**, *4*, 593–598.
34. Snook, G. A.; Chen, G. Z. The Measurement of Specific Capacitances of Conducting Polymers Using the Quartz Crystal Microbalance. *J. Electroanal. Chem.* **2008**, *612*, 140–146.
35. Doherty, E. M.; De, S.; Lyons, P. E.; Shmeliov, A.; Nirmalraj, P. N.; Scardaci, V.; Joimel, J.; Blau, W. J.; Boland, J. J.; Coleman, J. N. The Spatial Uniformity and Electromechanical Stability of Transparent, Conductive Films of Single Walled Nanotubes. *Carbon* **2009**, *47*, 2466–2473.
36. Hata, K.; Futaba, D. N.; Mizuno, K.; Namai, T.; Yumura, M.; Iijima, S. Water-Assisted Highly Efficient Synthesis of Impurity-Free Single-Walled Carbon Nanotubes. *Science* **2004**, *306*, 1362−1364.
37. Davis, V. A.; Ericson, L. M.; Parra-Vasquez, A. N. G.; Fan, H.; Wang, Y.; Prieto, V.; Longoria, J. A.; Ramesh, S.; Saini, R. K.; Kittrell, C.; *et al*. Phase Behavior and Rheology of SWNTs in Superacids. *Macromolecules* **2003**, *37*, 154–160.
38. Vigolo, B.; Coulon, C.; Maugey, M.; Zakri, C.; Poulin, P. An Experimental Approach to the Percolation of Sticky Nanotubes. *Science* **2005**, *309*, 920–923.
39. Green, M. J.; Parra-Vasquez, A. N. G.; Behabtu, N.; Pasquali, M. Modeling the Phase Behavior of Polydisperse Rigid Rods with Attractive Interactions with Applications to Single-Walled Carbon Nanotubes in Superacids. *J. Chem. Phys.* **2009**, *131*, 084901–084910.
40. Davis, V. A.; Parra-Vasquez, A. N. G.; Green, M. J.; Rai, P. K.; Behabtu, N.; Prieto, V.; Booker, R. D.; Schmidt, J.; Kesselman, E.; Zhou, W.; *et al*. True Solutions of Single-Walled Carbon Nanotubes for Assembly into Macroscopic Materials. *Nat. Nanotechnol.* **2009**, *4*, 830–834.
41. Syrgiannis, Z.; Gebhardt, B.; Dotzer, C.; Hauke, F.; Graupner, R.; Hirsch, A. Reductive Retrofunctionalization of Single-Walled Carbon Nanotubes. *Angew. Chem.* **2010**, *49*, 3322–3325.
42. Liang, F.; Alemany, L. B.; Beach, J. M.; Billups, W. E. Structure Analyses of Dodecylated Single-Walled Carbon Nanotubes. *J. Am. Chem. Soc.* **2005**, *127*, 13941–13948.
43. Strano, M. S.; Dyke, C. A.; Usrey, M. L.; Barone, P. W.; Allen, M. J.; Shan, H.; Kittrell, C.; Hauge, R. H.; Tour, J. M.; Smalley, R. E. Electronic Structure Control of Single-Walled Carbon Nanotube Functionalization. *Science* **2003**, *301*, 1519–1522.
44. Tu, X.; Manohar, S.; Jagota, A.; Zheng, M. DNA Sequence Motifs for Structure-Specific Recognition and Separation of Carbon Nanotubes. *Nature* **2009**, *460*, 250–253.
45. Zheng, M.; Jagota, A.; Semke, E. D.; Diner, B. A.; McLean, R. S.; Lustig, S. R.; Richardson, R. E.; Tassi, N. G. DNA-Assisted Dispersion and Separation of Carbon Nanotubes. *Nat. Mater.* **2003**, *2*, 338–342.
46. Liu, H.; Nishide, D.; Tanaka, T.; Kataura, H. Large-Scale Single-Chirality Separation of Single-Wall Carbon Nanotubes by Simple Gel Chromatography. *Nat. Commun.* **2011**, *2*, 309.
47. Krupke, R.; Hennrich, F.; Löhneysen, H. V.; Kappes, M. M. Separation of Metallic From Semiconducting Single-Walled Carbon Nanotubes. *Science* **2003**, *301*, 344–347.
48. Arnold, M. S.; Stupp, S. I.; Hersam, M. C. Enrichment of Single-Walled Carbon Nanotubes by Diameter in Density Gradients. *Nano Lett.* **2005**, *5*, 713–718.

49. Arnold, M. S.; Green, A. A.; Hulvat, J. F.; Stupp, S. I.; Hersam, M. C. Sorting Carbon Nanotubes by Electronic Structure Using Density Differentiation. *Nat. Nanotechnol.* **2006**, *1*, 60–65.
50. Yanagi, K.; Miyata, Y.; Tanaka, T.; Fujii, S.; Nishide, D.; Kataura, H. Colors of Carbon Nanotubes. *Diamond Relat. Mater.* **2009**, *18*, 935–939.
51. Hodge, S. A.; Bayazit, M. K.; Coleman, K. S.; Shaffer, M. S. P. Unweaving the Rainbow: a Review of the Relationship Between Single-Walled Carbon Nanotube Molecular Structures and their Chemical Reactivity. *Chem. Soc. Rev.* **2012**, *41*, 4409–4429.
52. Wunderlich, D.; Hauke, F.; Hirsch, A. Preferred Functionalization of Metallic and Small-Diameter Single Walled Carbon Nanotubes *via* Reductive Alkylation. *J. Mater. Chem.* **2008**, *18*, 1493–1497.
53. Burkin, A. R. *Production of Aluminium and Alumina*; John Wiley & Sons: New York, 1987.
54. Bayliss, C. R. Modern Techniques in Electrolytic Refining of Copper. *Electron. Power* **1976**, *22*, 773–776.
55. Harutyunyan, A. R.; Chen, G.; Paronyan, T. M.; Pigos, E. M.; Kuznetsov, O. A.; Hewaparakrama, K.; Kim, S. M.; Zakharov, D.; Stach, E. A.; Sumanasekera, G. U. Preferential Growth of Single-Walled Carbon Nanotubes with Metallic Conductivity. *Science* **2009**, *326*, 116–120.
56. Giordani, S.; Bergin, S. D.; Nicolosi, V.; Lebedkin, S.; Kappes, M. M.; Blau, W. J.; Coleman, J. N. Debundling of Single-Walled Nanotubes by Dilution: Observation of Large Populations of Individual Nanotubes in Amide Solvent Dispersions. *J. Phys. Chem. B* **2006**, *110*, 15708–15718.